

Morphology and Topography of Retinal Pericytes in the Living Mouse Retina Using In Vivo Adaptive Optics Imaging and Ex Vivo Characterization

Jesse Schallek,¹ Ying Geng,^{2,*} HoanVu Nguyen,^{1,3} and David R. Williams^{1,2,4}

¹Center for Visual Science, University of Rochester, Rochester, New York

²The Institute of Optics, University of Rochester, Rochester, New York

³Department of Biology, University of Denver, Denver, Colorado

⁴Flaum Eye Institute, University of Rochester, Rochester, New York

Correspondence: Jesse Schallek, Department of Ophthalmology, Center for Visual Science, University of Rochester, 601 Elmwood Avenue, Box 314, Rochester, NY 14642; jschallek@cvs.rochester.edu.

Current affiliation: *Corning Incorporated, Corning, New York.

Submitted: June 11, 2013

Accepted: September 4, 2013

Citation: Schallek J, Geng Y, Nguyen H, Williams DR. Morphology and topography of retinal pericytes in the living mouse retina using in vivo adaptive optics imaging and ex vivo characterization. *Invest Ophthalmol Vis Sci.* 2013;54:8237–8250. DOI: 10.1167/iovs.13-12581

PURPOSE. To noninvasively image retinal pericytes in the living eye and characterize NG2-positive cell topography and morphology in the adult mouse retina.

METHODS. Transgenic mice expressing fluorescent pericytes (NG2, DsRed) were imaged using a two-channel, adaptive optics scanning laser ophthalmoscope (AOSLO). One channel imaged vascular perfusion with near infrared light. A second channel simultaneously imaged fluorescent retinal pericytes. Mice were also imaged using wide-field ophthalmoscopy. To confirm in vivo imaging, five eyes were enucleated and imaged in flat mount with conventional fluorescent microscopy. Cell topography was quantified relative to the optic disc.

RESULTS. We observed strong DsRed fluorescence from NG2-positive cells. AOSLO revealed fluorescent vascular mural cells enveloping all vessels in the living retina. Cells were stellate on larger venules, and showed banded morphology on arterioles. NG2-positive cells indicative of pericytes were found on the smallest capillaries of the retinal circulation. Wide-field SLO enabled quick assessment of NG2-positive distribution, but provided insufficient resolution for cell counts. Ex vivo microscopy showed relatively even topography of NG2-positive capillary pericytes at eccentricities more than 0.3 mm from the optic disc (515 ± 94 cells/mm² of retinal area).

CONCLUSIONS. We provide the first high-resolution images of retinal pericytes in the living animal. Subcellular resolution enabled morphological identification of NG2-positive cells on capillaries showing classic features and topography of retinal pericytes. This report provides foundational basis for future studies that will track and quantify pericyte topography, morphology, and function in the living retina over time, especially in the progression of microvascular disease.

Keywords: diabetic retinopathy, neurovascular coupling, adaptive optics, capillaries, microvascular network

Retinal circulation is made up of various-sized vessels that deliver, exchange, and return a constant stream of metabolites and nutrients to the inner retina. The smallest of these vessels are the capillaries, which provide both metabolite exchange and act as the primary barrier between blood and surrounding tissue. Capillaries are composed of a thin tube of endothelial cells ensheathed by a vascular-associated cell type: the pericyte. Pericytes are a heterogeneous population of cells that send out long, dendritiform processes that ensheath the endothelial tube. Although pericytes are believed to belong to the same cell lineage as vascular smooth muscle cells, their intimate association with the endothelial basement membrane makes them phenotypically distinct from smooth muscle cells.¹ They distinctively are embedded in the vascular basement membrane of endothelial cells and contribute to the integrity of the blood retinal barrier.² Pericytes are found throughout the microvasculature of the body; however, they are found with exceptionally high microvessel coverage and topographic

density in the retina. The pericyte-to-endothelial cell ratio in the rodent retina is 1:1 to 1:3^{3,4} compared with 1:5 in the cerebral cortex,^{5,6} 1:10 in the lung, and 1:100 in skeletal muscle.⁷ This prominence suggests a unique functional and/or structural role for these cells in the retina, yet the full spectrum of functionality is still not completely understood. In the central nervous system, the high density of pericytes has been implicated in the role of maintaining the blood-brain barrier,^{8,9} providing vessel maturation and stabilization,^{10,11} vascular remodeling, and angiogenesis.^{12,13} Moreover, recent evidence suggests that they may regulate the fine control of neurovascular coupling at the level of small arterioles and even capillaries.^{14,15} The importance of this cell class is further appreciated given that several vascular diseases of the eye are linked with a profound loss of pericytes. For example, in diabetic retinopathy, a rapidly growing disease that is estimated to affect approximately 18 million people in the United States who have diabetes,^{16–19} pericytes are characteristically lost

with disease progression.^{20,21} Conversely, pericytes appear to have a lasting presence in conditions of hypertension, arteriosclerosis, and aging that exceeds that of their juxtaposed endothelial cells.^{3,4} The full natural history that leads to pericyte preservation or loss in retinal disease is still not fully understood.

Although many reports have identified the importance of this cell class in the retina, the vast majority of studies have examined these cells in vitro, or in postmortem histology. To date, the lack of in vivo investigation of retinal pericytes has been attributed to several technical obstacles that make imaging these small cells challenging. First, pericytes are small. Cell somas are approximately 7 μm and extend distal processes that are even smaller. Conventional retinal imaging techniques, such as flood illuminated fundus cameras and scanning laser ophthalmoscopes without adaptive optics correction, achieve only approximately 9 μm lateral resolution due to image blur imparted by the eye's optical aberrations. This poor resolution makes pericyte identification and characterization challenging in the living eye (Nguyen H, et al. *IOVS* 2013;54:ARVO E-Abstract 4878). Second, pericytes provide low optical contrast, thus making positive identification more difficult. Third, further complicating the above-mentioned obstacles, the eye is constantly in motion, with movement of more than tens-of-microns per image acquisition time, lasting seconds to minutes in duration. This ocular motion blurs fluorescent images that require long image acquisition times required for fluorescence imaging (Schallek JB, et al. *IOVS* 2012;53:ARVO E-Abstract 6831).

To overcome these obstacles, we have combined several technologies to study these cells in the living eye. To enable the subcellular resolution needed for this investigation we have deployed adaptive optics scanning laser ophthalmoscopy (AOSLO). Adaptive optics (AO) is a technology that corrects for both low- and higher-order aberrations that blur the retinal image,²²⁻²⁴ enabling the study of retinal cellular structure in vivo. Our group has recently developed a two-channel AOSLO designed to image the mouse retina that captures simultaneous reflectance and fluorescence images with resolution exceeding 0.7 μm ²⁵ and can provide field sizes less than or equal to 7° of visual angle (approximately 230 × 230- μm field). This resolution regime is sufficient to quantify the areal density of pericytes and resolve the morphology of pericytes in the living eye. We have outfitted the camera with a fluorescence channel that can collect the emitted fluorescence of transgenically labeled cells. To provide pericyte optical contrast, we image DsRed fluorescent pericytes from an NG2-labeled transgenic mouse model.²⁶ Finally, we incorporate subpixel image registration to correct for retinal motion and mitigate motion-blur.²⁷

Combining these approaches, we provide the first high-resolution images of fluorescent NG2 DsRed-positive pericytes in the mouse retina using two-channel AOSLO, adding to a growing number of fluorescent cellular structures observed in the living mouse eye.^{25,28,29} We further characterize the distribution of these cells by using a commercial confocal scanning laser ophthalmoscope (Heidelberg Spectralis HRA; Heidelberg Engineering, Inc., Carlstadt, CA). Finally, we validate in vivo cellular imaging by comparing the density, distribution, and morphology of NG2 pericytes in the mouse retina with ex vivo retinal flat mounts. This noninvasive, high-resolution approach demonstrates the ability to image retinal pericytes in their natural habitat, providing an important step in future longitudinal studies that will examine their role in disease, repair, and neurovascular control of the central nervous system microvasculature.

METHODS

Animals

Mice exhibiting red fluorescent pericytes under neural/glia antigen-2 expression (NG2 DsRed) were used to provide optical contrast in vivo. NG2 mice express an optimized red fluorescent protein variant (DsRed.T1) under the control of the mouse NG2 chondroitin sulfate proteoglycan 4 (*Cspg4*) promoter. Animals were purchased from Jackson Labs (Bar Harbor, ME) from stock Tg(Cspg4-DsRed.T1)1Akik/J. Mice hemizygous for the NG2 DsRed BAC transgene are viable and fertile and are phenotypically similar in appearance to their C57BL/6J counterparts. The weight range of NG2 animals was 13.5 to 30.0 g, within the range of age/sex-matched normal C57BL/6J mice (Jackson Labs). These mice are referred to as NG2 population hereafter. The NG2 model was developed by Nishiyama and colleagues, where it was demonstrated that in addition to oligodendrocyte progenitor cells, mature pericyte soma and processes strongly express DsRed fluorescence.^{26,30,31} Seven hemizygous mice were imaged at multiple intervals to confirm labeling was viable throughout adulthood. Animals were imaged between postnatal days 44 and 568 (1.5 months to 1.65 years of age). Mice expressing NG2 were successfully imaged in all imaging sessions; however, the quality and duration of imaging was also dependent on optical clarity of the eye, as the murine retina sometimes develops transient cataracts in response to anesthesia.³² Mice were housed in a vivarium with 12-hour light/dark cycle. Protocols conformed with the University Committee guidelines on Animal Resources at the University of Rochester, Rochester, New York. All procedures adhered to the ARVO Statement for the Use of Animals in Ophthalmic and Vision Research.

Animal Preparation

For imaging, mice were lightly anesthetized with intraperitoneal injection of ketamine/xylazine (100 mg/kg ketamine, 10 mg/kg xylazine), or with 2% isoflurane in an induction chamber. Once anesthetized, animals were positioned in a stereotaxic stage with a bite bar. The stage permitted adjustment of two axes of rotation, azimuth, and angle as well as *x*, *y*, and *z* translation allowing for precise alignment with the optical path of the AOSLO imaging beam. Movement of stage azimuth and angle allowed rotation of the mouse about the eye's pupil, permitting optical access across the retina. A rigid contact lens (0 to +10 diopter 1.55–1.7-mm base curve) was placed on the cornea to maintain hydration and optical quality (Unicon Corp., Osaka, Japan); 1% topical tropicamide and 2.5% phenylephrine (Alcon, Fort Worth, TX) were applied to dilate the pupil and freeze accommodation. Animals were maintained on 0.5% to 1.5% isoflurane anesthesia throughout the imaging session. A heat pad was used to maintain normal body temperature. Typical imaging sessions lasted 2 hours, after which animals were recovered and returned to their cage for use in subsequent imaging experiments.

AOSLO System Design

Detailed information regarding the implementation of the ophthalmic adaptive optics system is provided by the following manuscripts and reviews.^{22,33-35} The mouse AOSLO system used in this study is described in detail in Geng et al.²⁵ (see also Geng Y, et al. *IOVS* 2011;52:ARVO E-Abstract 5871) and a system diagram is provided therein. Briefly, three light sources are used for the following: wavefront sensing, 843-nm laser diode (Qphotonics, Ann Arbor, MI); near infrared reflectance imaging, 789-nm super luminescent diode (InPhenix, Liver-

more, CA); and fluorescence excitation, 514-nm Argon laser (Melles Griot, Albuquerque, NM). These fiber-coupled light sources were combined through a set of dichroic mirrors into a common optical path. Light sources are relayed through a reflective system to a resonance scanner operating at 15 kHz (Electro-Optical Products, Glendale, NY) that provides *x*-axis scanning. The *x*-axis scanned beam is projected to an orthogonal 25.5-Hz galvanometric scanner (GSI Group Corp., Bedford, MA). Combined, these scanners provided the Cartesian imaging raster of the scanned laser system. The raster beam was relayed to a large-stroke deformable mirror (DM97; ALPAO, Bivers, France), that corrected for higher-order aberrations (see below). The deformable mirror also enabled programmable defocus control, enabling axial focusing of the imaging beams permitting confocal imaging, described below. Light was then relayed through an achromatic doublet lens with 400- to 900-nm antireflection coating (Ross Optical, El Paso, TX).

Real-time adaptive optics correction was enabled by a feedback control loop between Hartmann-Shack wavefront sensor and the deformable mirror. The wavefront sensor was composed of a 7.8-mm focal length lenslet array (Adaptive Optics Associates, Cambridge, MA) focused on a Rolera XR camera (QImaging, Surrey, Canada). Wavefront spot patterns were corrected for displacement and focus and correction signal was relayed to the deformable mirror to provide diffraction-limited imaging.

Reflectance Imaging With AOSLO

After higher-order aberrations were corrected, the system provides diffraction-limited imaging in the mouse, resolving structures smaller than 0.7 μm .^{25,35} Fundus reflectance in the near-infrared (NIR, 789 nm) reveals high-contrast retinal structures that can be used for image registration to correct for eye motion.²⁷ We focused the NIR reflectance channel on the superficial retina, which revealed high contrast of the retinal capillaries. Acquisition allows frame capture of 640 \times 480 pixels (5° of visual angle) at a rate greater than 25 Hz. Field size was converted into dimensions in the retinal space by using a paraxial model of the adult C57BL/6 mouse, which approximates 34 μm per degree of visual angle.³⁶ Retinal reflectance images are digitized and stored on a computer hard drive for post hoc analysis.

NIR imaging provides continuous image capture that is far removed from the visual sensitivity of the mouse, which peaks in the UV-visible range (360–500 nm).^{37,38} Use of NIR wavelengths at power of 100 to 200 μW (at the cornea) provided high-resolution images below phototoxic levels.^{39–41} NIR light also permits visual function to be probed with minimal visible excitation, meaning the eye can be imaged in the dark-adapted state.

DsRed Fluorescence Imaging With AOSLO

A second optical channel was merged with the NIR light path to simultaneously excite DsRed fluorescence in the mouse eye. A 514-nm laser line was used to excite DsRed fluorescence (peak at 558 nm). Fluorescence emission was collected with two bandpass filters in series centered at 579 Δ 34 nm.⁴² Excitation/emission bands were carefully selected and optimized to ensure no excitation bleed-through into the fluorescent channel (Supplementary Figs. S1–S3). Power levels of 30 to 200 μW (at the cornea) were sufficient to provide a structural image of the cells. Sparse fluorescence from as few as 50 and as many as 2500 frames were averaged to produce a single fluorescent image; this corresponds to exposure times of 2 to 100 seconds. Fluorescent image stacks were registered

based on the estimated motion from the NIR reflectance channel.^{25,27}

Axial Resolution and Confocality of the AOSLO System

Both reflectance and fluorescence detection channels were read by Hamamatsu photomultiplier tubes (PMTs) optimized for the spectral bandwidth imaged (H7422-40 and -50; Hamamatsu, Shizuoka-Ken, Japan). A pinhole was placed in front of each PMT detector (1–2 Airy disc diameter 789-nm channel, 1.8–3.5 Airy disc diameter 579-nm channel) providing narrow optical sectioning. The axial resolution of the Rochester mouse AOSLO 6 μm ³³ not only provided exceptional axial sectioning capabilities but also increased optical contrast by providing information from a thin optical plane and rejecting thick volumetric blur. This feature is advantageous in the mouse retina, as it is approximately the same dimensional thickness as the primate retina, but the high optical power of the mouse eye makes the retina appear optically thick, covering approximately 30 to 40 diopters.^{35,36} Given this utility, we have previously demonstrated the optical sectioning that is possible in the mouse *in vivo*, showing ganglion cell axons, soma, and dendritic fields.²⁵ Longitudinal chromatic aberration (focus mismatch between reflectance and fluorescence channels) was manually adjusted by adjusting the excitation source and fluorescence pinhole position axially so that pericyte fluorescence in a given vessel stratification matched the vascular pattern in the NIR reflectance channel.

Image Registration

Because the retina is constantly in motion, even in the anesthetized animal, recorded AOSLO videos must be stabilized (image registration). We used custom software developed at the University of Rochester²⁷ based on image cross-correlation to a selected reference frame. In the two-channel imaging approach, we used the high signal-to-noise, high-contrast reflectance image (NIR wavelengths) as the registration signal to register the simultaneously captured fluorescence sequence. This was essential, as a single fluorescence frame contains low signal-to-noise and insufficient spatial information for robust cross-correlation-based alignment. Registration accuracy provides subpixel accuracy so that image resolution is limited by optics, not blur induced by eye motion.²⁷ Eye motion in the anesthetized mouse was primarily from heart rate and respiratory artifacts that create ocular movements on the order of tens-of-microns in the retinal image across the acquired video sequence. Correction for this ocular movement provided temporal stability to integrate fluorescence images over long periods of time.

High-Resolution, Motion Contrast-Enhanced Imaging of Vasculature Without Contrast Agents

The fast acquisition of AOSLO videos (25 Hz) reveals movement of highly reflective blood cells through the retinal microvasculature. The high spatiotemporal resolution of the AOSLO can resolve single blood cells that provide high backscatter of NIR light without contrast agents. This strategy avoids the need for repeated injections of extrinsic agents, such as sodium fluorescein, indocyanine green, microbeads, or acridine orange, which are short-lived in their effects, and may in some cases modify normal flow kinetics. Infrared AOSLO imaging also leaves the animals in a dark-adapted state, removing possible flow changes caused by a bright, visible excitation source^{43–45} or induction of photodamage. NIR imaging therefore mitigates toxic light exposure to the light-

sensitive retina, which is important for longitudinal studies in the same animals over time.

Near-infrared vascular contrast was optimized by motion contrast enhancement. In this strategy, the NIR image sequence (a series of N frames captured at 25 Hz) is evaluated for local motion contrast. In the stabilized retinal image, local motion is provided by the single blood cells as they traverse the vascular network. The method measures the temporal intensity variance of each pixel in a registered image sequence. It reports this optical variance as a measure of standard deviation value (Schallek J, et al. *IOVS* 2011;52:ARVO E-Abstract 6029 and Refs. 46, 47) and generates a grayscale map based on the variance value, where low variance is represented by dark pixels, and high variance by bright values. The temporal “flicker” induced by moving blood cells provides high pixel variance. Static structures show measurably less pixel intensity variance over time, and thus low motion-based contrast. Typically, collection of 25 frames (1-second acquisition) was sufficient to provide a strong motion-contrast signal. Motion-contrasted maps that indicate an active vascular system were overlaid on simultaneously collected fluorescent images of NG2 pericytes (above).

Wide-Field SLO Imaging

To obtain global information about NG2 expression over a larger field of view, we also imaged animals with Heidelberg Spectralis HRA (Heidelberg Engineering, Inc.). Anesthetized mice were mounted in a stereotaxic frame (as described above). The HRA Spectralis imaged the retina with the 55° field objective. Fluorescence was excited at 488 ± 2 nm laser line. A barrier filter at 505 nm provided long-pass fluorescence emission collection. This commercial configuration was suboptimal for DsRed excitation and emission, nevertheless was sufficient to provide strong fluorescence collection.

Ex Vivo Histology

At the termination of the longitudinal investigation, mice were killed by cervical dislocation after CO₂ asphyxiation. Standard histological procedures were used to prepare the retina flat mount. Briefly, eyes were immediately removed and placed in 4% paraformaldehyde in phosphate buffer (pH 7.2). A slit was made near the ora serrata to allow fixative to enter the globe. Tissue was fixed for approximately 2 hours. Under a dissecting microscope (Olympus VM; Olympus, Tokyo, Japan) the anterior chamber was then removed by making a slit at the cornea, from which the lens could be extracted. The lens was removed and dissecting scissors were used to remove the anterior segment from the posterior globe with a continuous cut along the ora serrata. The retina was then carefully teased away from the retinal pigmented epithelium using blunt forceps or stiff bristles. Four radial relief cuts were placed, and the retina was flat mounted on a microscope slide. Vectasheild (Vector Laboratories, Burlingame, CA) was applied and the specimen was cover-slipped. Histology was performed on six eyes from three animals; one retinal flat mount became folded in histological preparation and could not be included in topography measurements.

Microscopy

Postmortem microscopy was performed on epifluorescent and confocal microscopes. Epifluorescent images were acquired with an Olympus BX53 microscope (Olympus) using NeuroLucida software (MicroBrightField, Inc., Colchester, VT). Excitation and emission were filtered using a Texas Red filter set that closely matched the excitation/emission specs with

that of the optimized variant of DsRed (Semrock, Inc., Rochester, NY). Large contiguous montages of more than 36 image fields were captured at $\times 20$ magnification (air objective). Captured fields of view at this magnification were manually stitched using Adobe Photoshop CS5.1 (Adobe Systems, Inc., San Jose, CA). Images at the same focus plane were montaged to produce a single high-resolution image. Several imaging planes focused on different planes of the inner retinal vasculature were combined in an entire flat mount image stack (high-resolution stacks available on request, see Supplementary Fig. S4).

Confocal images were acquired with a Zeiss, LSM 510 Meta using ZEN software (Carl Zeiss, Oberkochen, Germany). Air and oil objectives $\times 5$ to $\times 100$ magnification were used to capture wide-field and high-resolution images; 514-nm laser line was used for DsRed excitation, in conjunction with long-pass dichroic and selectable band-pass filters to maximize DsRed emission throughput.

Ex Vivo Cell Quantification

Cells positive for NG2 were classified into two subpopulations for analysis. Cells on vessels smaller than 7 μm were classified as capillary pericytes, those on larger vessels were classified as arteriole/venule NG2 vascular mural cells. For capillaries, cell counts were performed in multiple depths of focus, which ensured that every pericyte was counted, regardless of retinal capillary stratification (the murine retinal circulation has at least three vessel stratifications⁴⁸). Manual counts were performed on retinal flat mounts using custom scripts written in Matlab (Natick, MA), and with publically available ImageJ software (National Institutes of Health, Bethesda, MD). Cells were counted in Cartesian space relative to the optic disc. Each cell position was recorded as a vector (x, y position) relative to the center of the optic disc ($x = 0, y = 0$). This complete data set was then segmented in 100- μm radial bins relative to the disc, yielding cell-density counts as a function of radial eccentricity from the optic disc. This approach allowed for complete analysis of cell density in the horizontal and vertical meridians, as well as a general report of density as a function of eccentricity. Due to necessary relief cuts for flat mount preparation, gaps in retinal area were corrected for by directly measuring the area of retina measured in each radial annulus.

Three-Dimensional Rendering

Several supplementary figures showing three-dimensional (3D) volume renderings were produced by processing confocal stacks (captured in vivo with AOSLO or ex vivo using confocal microscopy) using publically available ImageJ software (National Institutes of Health) with 3D viewer plugin developed by Schmid et al.⁴⁹

RESULTS

Fluorescent NG2 Pericytes Imaged In Vivo With Adaptive Optics Retinal Imaging

Adult mice with the NG2 DsRed fluorescent transgene showed fluorescent cells in close apposition with the retinal vessels. High-resolution images captured with the fluorescence channel of the AOSLO revealed distinct cell soma with extensive dendritiform processes surrounding arterioles, venules, and capillaries. To verify the apposition of these cells to the vascular network, we performed simultaneous motion contrast imaging using NIR light (see Methods section). Motion-contrasted video sequences revealed a map of active blood

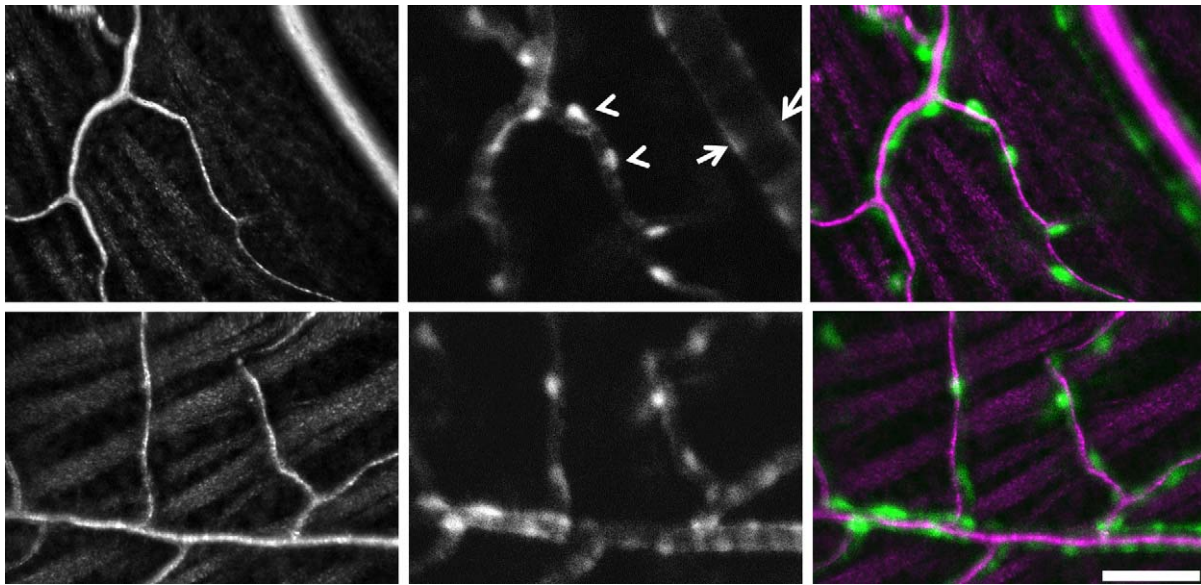


FIGURE 1. In vivo imaging of vascular perfusion and NG2 DsRed cells captured with AOSLO. *Left:* Images are from two animals showing the most superficial vascular stratification of the inner retina. Traces of the retinal nerve fiber bundles can be seen in surrounding tissue. Vascular images are motion contrast-enhanced with bright pixels showing strong temporal variance, indicative of moving blood cells within the active vascular circulation. *Middle:* Simultaneous fluorescence channel captured DsRed fluorescence. NG2 cells are seen in close apposition to the vasculature. Vessels smaller than 6 μm showed sparse and evenly distributed cells consistent with the morphology of pericytes (*arrowheads*). Vessels larger than 10 μm showed dense clustering of cells consistent with pericyte or vascular mural cell coverage of arterioles and venules (*arrows*). *Right:* A pseudocolor merged image of vascular motion contrast (*magenta*) and NG2 fluorescence (*green*). *Scale bar:* 50 μm .

perfusion as red and white blood cells moved through the microvascular network. These perfusion maps colocalized with simultaneously acquired fluorescent pericyte images. Fluorescent cell somas were round in shape and were adherent structures surrounding the vascular lumen. Using this two-channel approach, we rarely observed occurrences of positively labeled cells that did not associate with the vascular plexus. Of these rare occasions, it was often the case that NG2 cells were associated with a capillary on a slightly deeper or superficial imaging plane as dual defocus correction was needed to overcome the appreciable longitudinal chromatic aberration in the mouse when imaging 789-nm and 514-nm channels simultaneously. NG2 cells were distributed throughout the adult retina from cells on the vessels emerging from the optic disc to the smallest vessels in peripheral imaging fields greater than 30° of visual angle from the optic disc. In retinal

fields acquired across these eccentricities, we observed a morphological difference between cell appearance on capillaries, arterioles, and venules.

On retinal capillaries, which generally lack vascular smooth muscle cells, NG2 cells showed round cell soma with close apposition to the capillary endothelium. Cells on capillaries exhibited a sparse spacing pattern with minimal clumping or cell overlap along the capillaries (Fig. 1, *arrowheads*), features consistent with the morphology of retinal pericytes from previous reports.^{1,4,20} Fluorescence intensity was highest in cell soma with weaker fluorescence in distal processes stretching between adjacent pericytes on the same capillary. An image montage of multiple high-resolution fields is combined from both motion-contrast and fluorescence imaging channels of the AOSLO (Fig. 2). For comparison, vascular anatomy is compared with a conventional fundus image of the

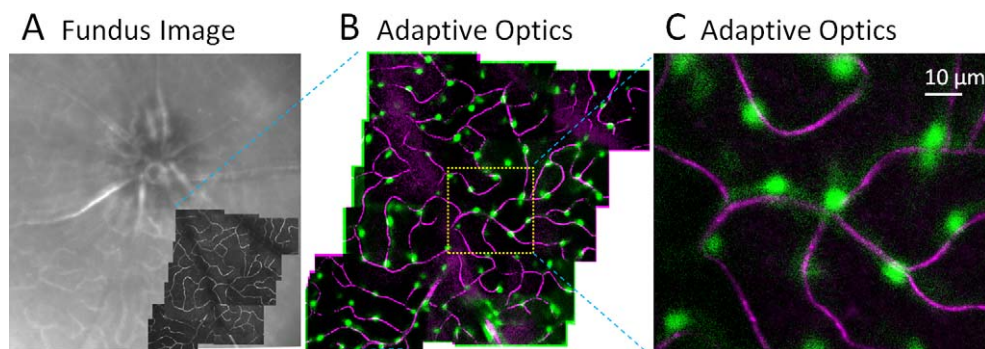


FIGURE 2. Simultaneous imaging of vascular perfusion and pericytes in vivo. (A) Wide field HRA Spectralis image shows approximately 30° field of mouse retina. Superimposed (*dark*) are motion-contrast AOSLO fields revealing capillary perfusion with micron-level resolution. (B) In vivo, two-channel imaging using AOSLO. Channel 1 collects NIR motion contrast that reveals capillary perfusion (*magenta*, moving blood cells). Channel 2 simultaneously images DsRed fluorescence (pericytes, *green*). (C) 5° AOSLO field shows the association of pericytes with perfused capillaries. Montage is from a single capillary stratification.

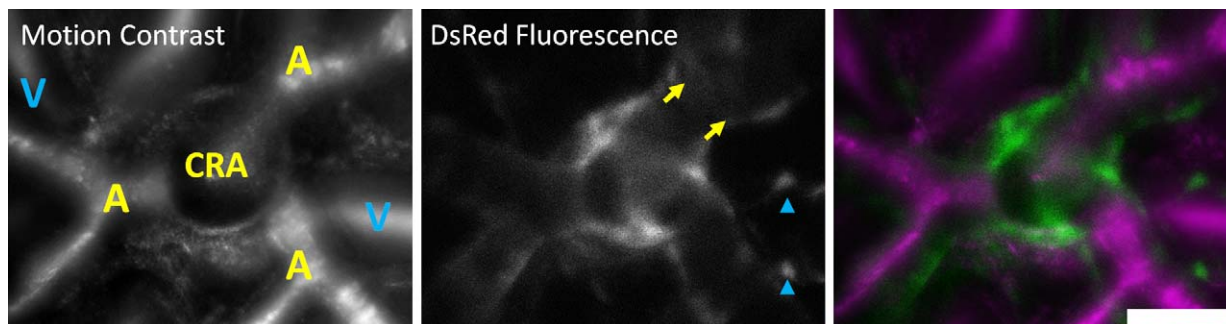


FIGURE 3. NG2-positive cells at the emergence of the central retinal artery. *Left:* AOSLO images revealed motion-contrasted images of blood flow at the optic disc. The emergence of the central retinal artery (CRA), the point source of all blood flow to the inner retina can be seen en face. Arterioles (A) branching from this point are labeled in *yellow*. The venous return from several venules (V) is labeled in *blue*. Vessels were identified in AOSLO videos by the direction of blood flow. *Middle:* DsRed fluorescence showed punctate labeling on venules (*blue arrowheads*), relatively denser labeling on arterioles (*yellow arrows*), and a circular band around the circumference of the central retinal artery. *Right:* The merged image shows the abutting fluorescent structures (*green*) surrounding the central retinal artery and diversion of the retinal vasculature (*magenta*). *Scale bar:* 50 μm .

retina at left. Few capillaries can be seen in the conventional “red-free” image (488-nm illumination). High-resolution motion-contrasted capillaries from a scleral capillary stratification are superimposed for comparison. The combined high-resolution and motion-contrast enhancement provide a better means for high resolution of the capillary network (magenta). In this montage view, the roughly uniform density and distribution of capillary pericytes is apparent. A single field of view (right) shows that NG2 cells colocalize with the capillary endothelium.

On venules and arterioles, there was dense cell labeling. The density and proximity of adjacent cells on venules and arterioles made single-cell segmentation difficult, as the dendritic processes of one cell had significant overlap with its neighbors. This observation was corroborated by *ex vivo* histology (below). Given the close packing density on arterioles and venules, coupled with the 6- μm axial resolution of the AOSLO, larger arterioles and venules in the mouse approximately 30 μm in diameter could be optically bisected when imaging en face (vascular axis parallel with imaging plane). This approach revealed two separate vascular walls on either side of the vascular lumen (Figs. 1, 3, arrows). We also were able to resolve NG2 cells on large vessels orthogonal to the imaging plane. The central retinal artery, which feeds the entirety of the retinal circulation, emerges from the optic nerve so that the bore of the vessel can be imaged en face (vessel axis is orthogonal to imaging plane). We imaged a strong density of NG2-positive cells on the emergence of the central retinal artery, but little in the surrounding optic disc space (Fig. 3). At this plane of focus, still within the neural retina, this vascular ring is indicative of vascular smooth muscle rather than oligodendrocyte or astrocyte progenitors, which are expected to arise in an approximately 0.6-mm deeper focus within the retrobulbar space.⁵⁰

Empirically, fluorescence labeling appeared stronger and more uniform on arterioles than on adjacent venules (Fig. 3). This feature is consistent with greater mural cell density on arterioles than on venules, likely due to the greater density of NG2 cells on arterioles (see histology, below). A dynamic, through-focus of this location is offered in Supplementary Figure S8. As a control measure to ensure that fluorescent light collected was not an artifact of excitation bleed through or intrinsic fluorophores, we imaged NG2-hemizygous littermates with the same excitation light-and-gain setting on the PMT. Hemizygous littermates showed no fluorescence in the DsRed band, background levels were no different from noise values acquired in positive fluorescence animals (Supplementary Fig.

S1). This ensured that the fluorescence detected was from the *cspg4*-linked transgene.

Depth Resolved Imaging of NG2 Pericytes

Using the confocality of the mouse AOSLO (approximately 6 μm^{25}) we optically focused through the retina from the nerve fiber layer (inner retina) to the photoreceptor layer (outer retina). The resultant image stack (Z-stack) recorded sequential frames progressively from vitread to scleral focal depths. Using this strategy, we observed three distinct capillary stratifications within the retinal circulation. Figure 4 shows capillary stratifications at three different depths within the same retinal field. A complete image stack is shown in Supplementary Figure S6 with both vascular and pericyte planes shown simultaneously. This stack was also rendered as a two-channel, 3D volume in Supplementary Figure S7. This result *in vivo* is consistent with postmortem histological findings in the mouse, which has stratifications in the nerve fiber layer, inner plexiform layer, and outer plexiform layer.^{48,51}

The simultaneously collected fluorescence in the second AOSLO channel showed NG2-positive cells colocalized with capillary paths in each of these stratifications. The 6- μm axial section of the confocal system provided means to identify fluorescently labeled cells with same *x-y* position, at different depths (*z* position). Using this strategy allowed for accurate *in vivo* quantification of pericyte density, as superficial pericyte soma did not obscure underlying cells on a deeper stratification (e.g., green arrow in Fig. 4).

NG2 Cells Imaged With HRA Spectralis

NG2 expression was also observed with wide-field scanning laser ophthalmoscopy. Wide-field images showed a relatively uniform density of NG2-positive cells on vessels throughout the murine retina. Cells on arterioles and venules were labeled from the optic disc to the far periphery (Fig. 5). We frequently observed a higher cell density around arteriole and precapillary arteriole branch points. Densities of NG2-positive cells were observed on the arterioles and venules, as well as strong abutting structures at confluence of vessels at the optic nerve head. Strong labeling was observed in several animals at the locus of the vestigial persistence of the hyaloid body at the optic disc (Fig. 5A, bottom two fluorescent images). Areas of punctate NG2 cells were observed in areas of known capillary beds between larger arterioles and venules. However, because the SLO provides lower image resolution, individual capillaries

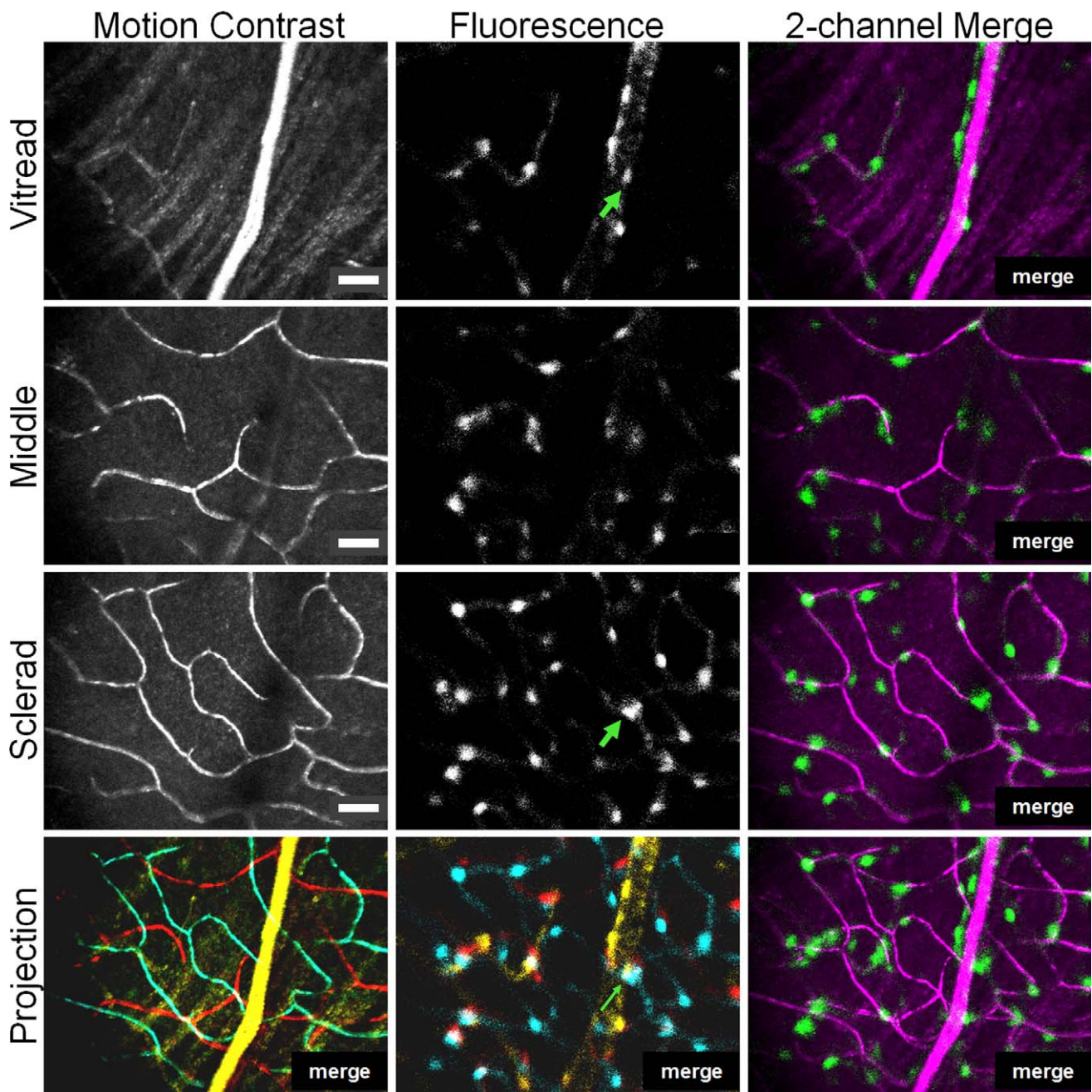


FIGURE 4. Depth-resolved imaging of retinal pericytes in three capillary stratifications. The confocality of the AOSLO enables thin optical sectioning along the optical axis ($Z = 6 \mu\text{m}$). The same retinal field was imaged at vitread (near retinal nerve fiber layer), middle (near inner plexiform layer), and sclerad (near outer plexiform layer). Three distinct capillary stratifications were observed with infrared motion contrast (*left*). Simultaneously captured DsRed fluorescence (*middle*) showed pericytes at each stratification. Pericytes colocalized with vessels at each of the three microvessel stratifications (*right*, vessels are *magenta* and NG2 cells are *green*). The *bottom row* shows a pseudocolored maximum projection image where *yellow* = vitread, *red* = middle, and *cyan* = sclerad planes. The tristratified capillary network also shows tristratified pericyte coverage. The optical sectioning provided by AOSLO enables disambiguation of two overlapping NG2 cells en face (*green arrows*) that would otherwise be interpreted as one cell in a nonconfocal instrument. *Scale bars*: $25 \mu\text{m}$.

cannot be reliably seen with the same resolution offered with AOSLO imaging, as capillaries generally exceed the resolution wide-field SLO. Cell counts were not performed in wide-field images because insufficient resolution precluded accurate identification of all cell bodies in the imaged field. The coarse axial point spread function of the wide-field SLO on the order of tens-of-microns did not provide sufficient axial resolution to segregate individual capillary stratifications, as fluorescent cell intensity was integrated through most of the neural retina. HRA

imaging did however provide a quick snapshot of the global health of NG2 cells across the retina (Fig. 5) and could target areas of interest for high-resolution AOSLO imaging.

NG2 Fluorescence Is Maintained Throughout Adulthood

The NG2 transgene is noted to persist in mature vascular mural cells (pericytes) in the adult brain.^{9,52} In the retina, we

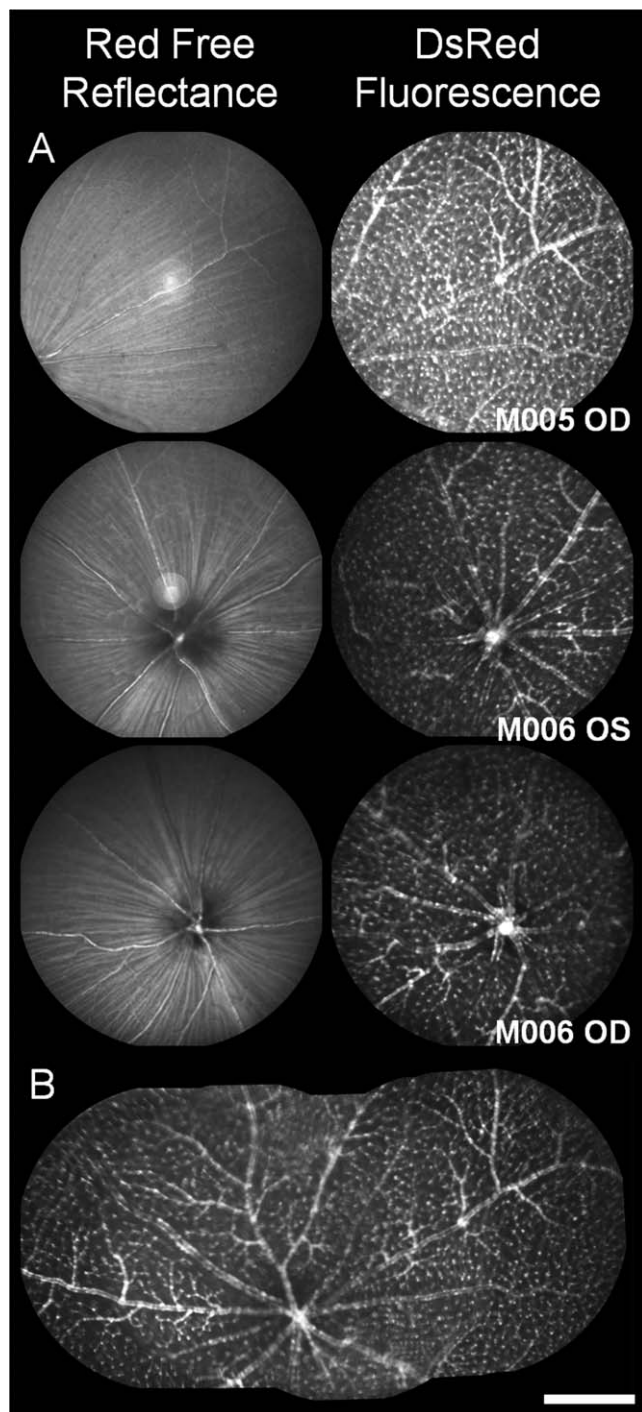


FIGURE 5. Red-free and NG2 fluorescence images from HRA Spectralis. (A) Red-free imaging in mice shows weak contrast of vessels, especially smaller microvessels. Fluorescence imaging of the same location shows density of NG2 DsRed cells surrounding the vascular network. DsRed provides enhanced contrast of vascular structures that are difficult to resolve in red-free imaging. (B) Q wide field composite image shows a mosaic representation of the optically accessible fields in the HRA Spectralis spanning more than 100° of visual angle in mouse 005. Data are from three retinas in two mice, M005 and M006. Scale bar: 15° of visual angle, or approximately 500 μ m.

observed robust NG2 fluorescence throughout the normal life span of the adult mouse. The youngest animal we imaged was postnatal day 44 (P44 = 0.12 years of age), which was considered a young adult based on proximity to fecundity.

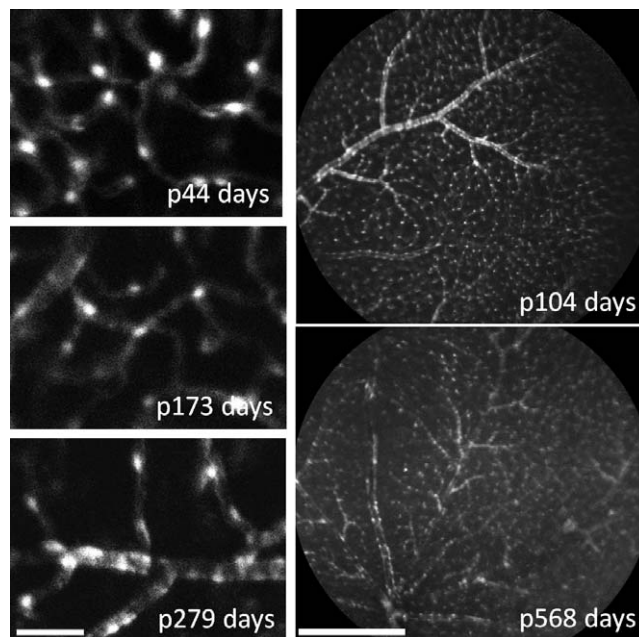


FIGURE 6. NG2 DsRed fluorescence remains in retinal mural cells throughout adulthood. *Left:* Pericytes exhibited strong fluorescence as imaged with AOSLO from postnatal day 44 to 279. Images were acquired with the same excitation power and camera gain settings. *Right:* HRA Spectralis imaging also showed strong labeling detection across the retina in intermediate-to-late adulthood. AOSLO images, scale bar: 50 μ m or approximately 1.5° of visual angle. HRA scale bar: 500 μ m or 15° of visual angle.

Earlier time points were not imaged *in vivo* due to the rapid and nonlinear development of the mouse optics from birth to P40.³⁶ The oldest mouse we imaged was P568 (1.65 years of age, after which it was killed for *ex vivo* morphology). The oldest animal showed strong fluorescence both *in vivo* and *ex vivo*. Empirically, fluorescence intensity was similar between young adults to very old animals. We did not quantify fluorescence intensity; however, the same laser intensity and detection gain settings with adaptive optics imaging yielded fluorescence images of similar quality and brightness (Fig. 6), suggesting NG2 expression remained active (this was also corroborated with *ex vivo* fluorescence intensity, see below). In animals across the range we examined, fluorescent NG2 cells were observed surrounding arterioles, venules, and capillaries.

Ex Vivo Cell Morphology

To confirm NG2-positive labeling, several animals were killed to examine fluorescence and cell morphology with conventional microscopy. Five flat-mounted retinas from three animals confirmed NG2-positive labeling seen *in vivo*. Wide-field SLO images were used to identify retinal orientation, and overlays near the optic disc showed good agreement between cell patterns observed *in vivo* with those seen in the flat-mount preparation (Supplementary Fig. S9).

Epifluorescent and confocal imaging revealed strong NG2 DsRed fluorescence. Consistent with cell morphology identified *in vivo*, NG2 cells colocalized to the retinal vasculature and showed different cell morphology on arterioles, venules, and capillaries (Fig. 7). Arterioles showed a cellular banding pattern. At higher magnification, banding appearance was produced from the directionality of cell dendritic processes that wrap the girth of the vessel. (Fig. 7; Supplementary Figs.

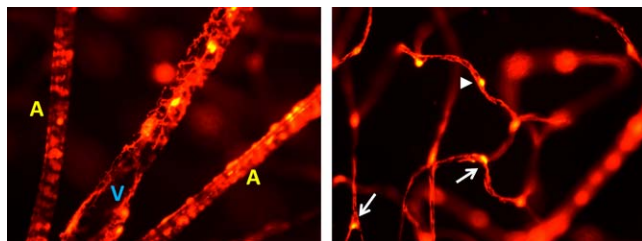


FIGURE 7. *Left:* Radial pattern of arterioles and venules near the optic disc. A single venule (V) is seen in the middle flanked by two arterioles (A). Venules are identified by their mural cell morphology that showed more sparse NG2 vessel coverage with cells showing a stellate shape. Both soma and dendritic processes can be identified. Two arterioles can be seen flanking the venule. Arterioles throughout the retina showed a banded appearance indicative of mural cells with densely packed soma and processes that had a directionality wrapping around the circumference of the vessel. *Right:* Morphology of NG2 cells on capillaries showed an evenly distributed appearance with minimal overlap. Somas often protruded from the capillary, with processes incompletely covering the capillary endothelium. Processes stretched tens of micrometers between neighboring pericytes. Soma were often located at capillary branch points (*arrows*), whereas others were found in the middle of capillary branches (*arrowhead*). Images are from an NG2 mouse 9 months old, and are representative of each retina we observed regardless of age postnatal day 44 to 568. Image fields were captured at $\times 40$ magnification.

S10, S11) This finding in the retina is consistent with smooth muscle and pericyte anatomy defined with scanning electron microscopy⁷ and with immunohistochemical fluorescence microscopy.⁵³ Venules showed a more sparse coverage of NG2 cells than that of their arteriole counterparts. Individual cells were stellate in shape with strongly labeled cell soma and clearly demarcated dendritiform processes. This sparse patterning was sometimes observed in vivo at large venules near the optic disc (Figs. 3, 7). Distinct from arterioles, NG2 cells did not show banding from dendritiform processes encircling the girth of the venules (Fig. 7; Supplementary Fig. S10). This labeling pattern is consistent with mural cell labeling on venules.^{1,53}

On capillaries, NG2 cells showed a sparse and distributed pattern along the capillary length. Unlike patterning on arterioles and venules, there was minimal clumping on capillaries. Cell somas were strongly labeled with long dendritiform processes that stretched between adjacent cells along the capillary endothelium. The distal processes of NG2 cells showed dense, but incomplete coverage of the vessel endothelium (Fig. 7, right; Supplementary Fig. S10). This characteristic is consistent with pericyte morphology reported in other studies to cover more than 70% to 85% of the capillary wall,^{5,54} and distinguishes NG2 cells as pericytes rather than endothelial cells that provide complete coverage of the vascular lumen. Cell soma on capillaries were round in shape,⁵⁵ further distinguishing them from the elongated soma shape seen in endothelial cells.⁴⁻⁶ On capillaries, we observed a tendency for pericyte soma to localize at capillary branch points with processes extending to both branches, resembling a “Y-shape,” described in several reviews.^{1,53} In addition to their position on capillary junctions, pericytes also were found solitary along straight, single branches. These locations could be resolved both in vivo (Figs. 1-3) and ex vivo (Fig. 7).

Ex Vivo Cell Density

Flat mounts from three animals, five retinas showed the same heterogeneous patterning of cells on arterioles, venules, and capillaries. In the retinal circulation, capillary pericytes (NG2

cells found on vessels $< 7 \mu\text{m}$) showed a relatively even distribution per retinal area as a function of retinal eccentricity. In four complete retinal flat-mounts from two animals, we counted every visible pericyte. Flat mounts were in exceptionally good condition, with average retinal area of 15.3 mm^2 of retinal tissue. The typical mouse eye contains roughly 15.6 mm^2 of retinal area,^{15,56} meaning our counts encompassed more than 98% of the complete mouse retina. Pericytes were counted in a series of focal planes to avoid missing deep or superficial pericytes, or pericytes that were in the same retinal position, but at different depths (Supplementary Figs. S4, S5). On average, there was agreement in total capillary pericytes per retina (7654 ± 403 , mean ± 1 SD). Cells were also counted as a function of retinal eccentricity from the optic disc (Fig. 8). NG2 pericytes on capillaries were distributed evenly across the retina as a function of eccentricity. This was especially true at retinal eccentricities beyond $300 \mu\text{m}$ where the retinal area is not dominated by arterioles and venules larger than $7 \mu\text{m}$. The average NG2 pericyte density on capillaries was 515 ± 94 cells/ mm^2 at eccentricities between 300 and $2300 \mu\text{m}$ (Fig. 8, data from five retinas). A complete list of cell counts in five retinas is provided in Supplementary Table S1.

Conversely, NG2 cell counts on arterioles and venules was greatest at the disc and waned at greater eccentricity as vascular branch structures became progressively smaller. The density estimate near the disc is expectedly high because it represents the high density of NG2 cells on retinal arterioles and venules, which are at highest ratiometric density per retinal area near the disc. Cells on large vessels resembled the known morphological phenotype of vascular smooth muscle cells (Fig. 7, Supplementary Fig. S11).

DISCUSSION

Summary

In this report, we have shown the first images of NG2 cells in the living eye. Using two in vivo imaging modalities, AOSLO and a commercial wide-field SLO, we have noninvasively imaged retinal pericytes with positive NG2 fluorescence. Imaging this cell population in the living eye provides a first step toward the goal of understanding the role of pericytes in health and disease without requiring postmortem histology. There are several advantages to studying pericytes in the living eye: (1) The same cell population can be tracked and studied over the course of disease onset and progression, increasing the sensitivity of studies examining pericyte pathology over time. (2) The noninvasive approach allows study of vascular-associated pericytes in blood-perfused tissue. Because pericytes dynamically interact with an active blood perfusion system, this advancement may revolutionize our understanding of the association of pericytes and blood flow. (3) Pericyte morphology and size may be more accurately represented in vessels that are unfixed and in normal pressure regimes rather than in histologic sampling where cell morphology often shows a shrunken and collapsed vascular network (see Supplementary Figs. S10, S11). (4) Studying both the laminar and lateral distribution of pericytes in the retinal circulation offers an advantage over histological study, preempting the need to correct for histological artifacts, such as flat-mount cuts, warping, and tissue distortion. Taken together, this work provides the basis for forthcoming studies that may systematically examine the anatomy, physiology, function, ontogeny, progeny, and transformative role of pericytes in the same animal over time.

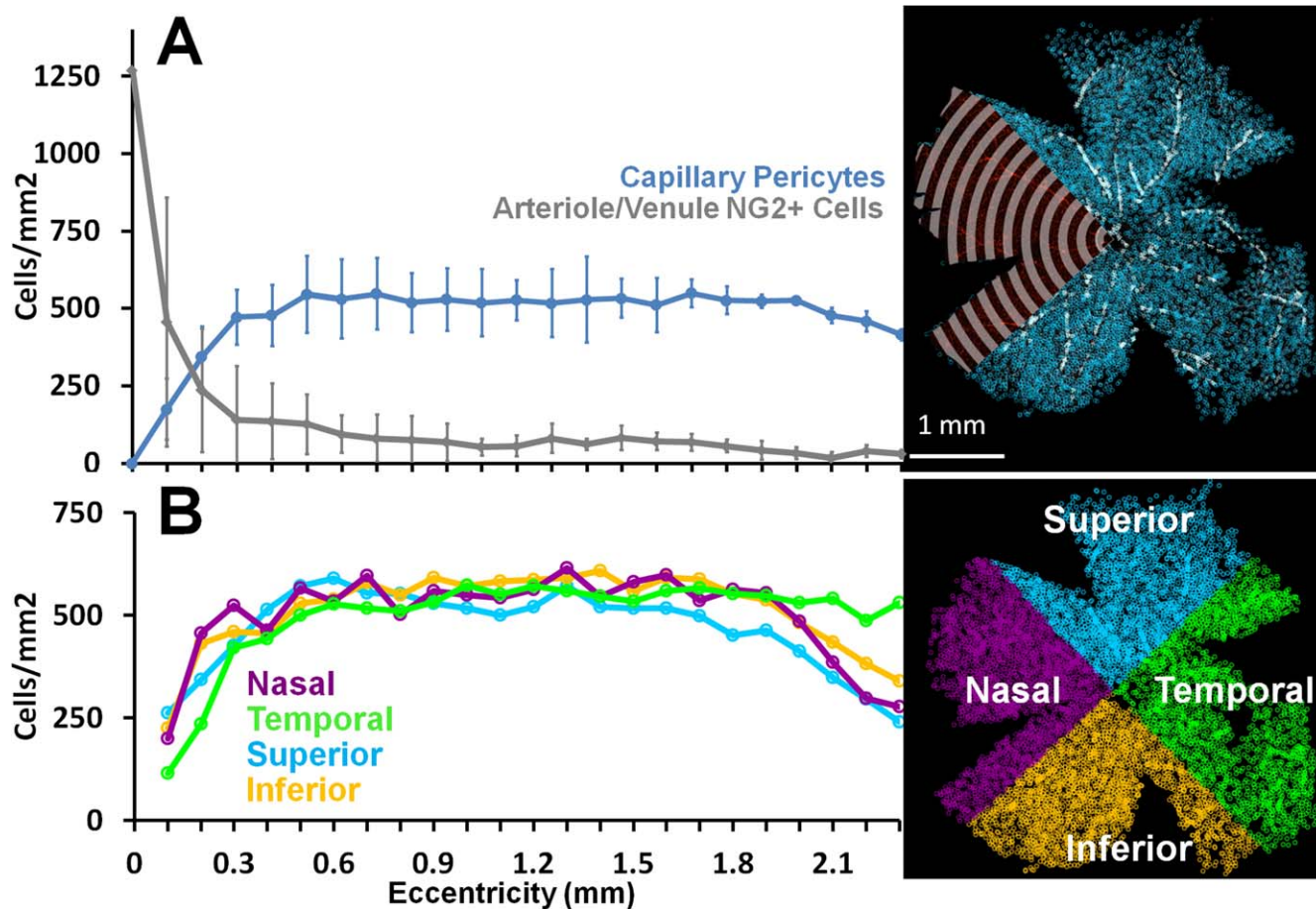


FIGURE 8. The density of capillary and A/V pericytes per retinal area are plotted as a function of retinal eccentricity. (A) NG2 pericytes were manually identified and counted from retina flat mounts. More than 36 high-magnification fields were tiled in Cartesian space and cell position was recorded relative to optic disc (coordinate space = 0,0). Radial bins every 100 μm were used to count pericytes in all directions from the optic disc (a sample analysis overlay is shown in a single quadrant for clarity, *top right*). Two populations of pericytes were counted: capillary pericytes (*blue*) were defined as pericytes on vessels smaller than 7 μm , arteriole/venule pericytes were on vessels 7 μm or larger (A/V, *gray* data). Cell counts were performed in multiple focal planes, which ensured that all pericytes were counted, regardless of depth of view. Capillary pericytes are evenly distributed in regions not dominated by large A/V density near the disc. Data shown include mean of five retinas from three animals ± 1 SD. (B) Capillary pericytes were quantified as a function of cardinal direction. Density estimates in four quadrants are shown to have the same general distribution characteristics in all retinal directions relative to the disc. Data in (B) are average of four retinas from two animals.

Imaging In Vivo

The morphology of fluorescent cells observed in vivo is consistent with the classic features of pericytes examined with conventional microscopy. On capillaries, we resolved NG2 cells with strongly labeled soma and weaker, but extensive, dendritiform labeling. This observation is also consistent with NG2 pericytes in the brain, where it was demonstrated that both pericyte soma and processes express DsRed fluorescence.^{26,30,31} Using the power levels and durations defined in the methods section, we did not observe photobleaching of the Tg fluorophore when examining in vivo images, nor was there evidence of photobleaching of AOSLO fields when examining ex vivo tissue.

Using two-channel AOSLO imaging, we verified the NG2-positive cells positively colocalized with perivascular structures. To do this, we used a novel methodology to simultaneously image intrinsic movement of single blood cells (vascular perfusion) and emitted fluorescence of extrinsically labeled DsRed pericytes. The two-channel AOSLO approach revealed that positively labeled cells exclusively colocalized to the vascular network. For this reason, and several discussed below, it is unlikely that these labeled cells represent glial

progenitor cells that would be found in areas between the vascular network and not on capillaries themselves.^{26,57,58}

AOSLO imaging also provided the necessary resolution to visualize the 3D organization of the retinal circulation. The holangiotic retina of mice (and primates) contains multiple stratifications of capillaries, collectively referred to as the inner retinal circulation.^{48,59} In the mouse, there are three stratifications of capillaries that generally project to the ganglion cell/nerve fiber layer, inner plexiform layer, and outer plexiform layer. The 6- μm axial section of the AOSLO²⁵ provided adequate optical sectioning and separation to distinguish each of these three distinct stratifications in the mouse retina (Fig. 4; Supplementary Figs. S6, S7). To our knowledge, this combined submicron lateral resolution and 6- μm axial resolution has never been achieved in the living eye to image the fluorescent morphology of pericytes in each of the capillary stratifications. This approach offers a unique opportunity to not only study the distribution of pericytes as a function of retinal eccentricity, but also in axial depth within the living eye.

We also show the potential to image pericytes using commercially available devices. The excitation laser line for the HRA Spectralis was at 488 nm, and although off the excitation peak of DsRed, was still sufficient to provide DsRed

fluorescence in the absorption tail of the fluorophore. Wide-field SLO imaging provided for global approximation of NG2 cell density across a wide retinal field. Analysis of this type may provide important information regarding global pericyte dropout in the course of diseases, such as diabetic retinopathy, that are known to affect pericyte density. Compared with the high-resolution approach of AOSLO, we found that commercial SLO resolution (both axial and lateral) was insufficient to provide reliable cell count estimates. Dense aggregates of cells exceeded the Rayleigh criterion for distinguishing two adjacent cell soma using HRA Spectralis. Moreover, we found that pericytes in superficial stratifications could occlude cells at the same eccentricity in deeper layers, thereby providing an underestimation of cell density per retinal area. Nonetheless, we found wide-field imaging may provide a useful tool for rough, global estimates of cell distribution. Moreover, the combined use of both the wide-field capabilities of HRA in conjunction with the high-resolution imaging of AOSLO may provide an integrated picture of the global and local health of retinal cell types, which, to date, have never been combined in the living retina.

Morphology of Observed Vascular Cells

Although several pericyte markers have been characterized, there is no single label that unequivocally identifies pericytes versus vascular smooth muscle cells, oligodendrocyte progenitors, or macrophages.⁵³ By morphological definition, pericytes must share an adjacent basement membrane with vascular endothelial cells, requiring electron microscopy for absolute characterization. However, most investigators agree that this approach is impractical for system-level investigation. In this report, we use a combination of NG2 labeling and cell morphology to identify pericytes in the retina, a model that has been used in the past to study pericytes in the brain.³⁰ NG2 is one of several validated pericyte markers.^{53,60-62} Morphology of NG2 cells in the microvasculature is consistent with pericytes identified by other means, such as immunocytochemistry^{9,52,55} and trypsin digests.^{4,20,63} In particular, NG2 cells on retinal capillaries generally lack vascular smooth muscle cells,^{12,14,64} and thus the identified cells we observe on vessel diameters smaller than 7 μm are morphologically and categorically indicative of capillary pericytes. Confocal and epifluorescent microscopy confirmed dense, but incomplete process investment in the endothelial membrane (Supplementary Fig. S10). We did not quantify the ratiometric coverage of capillary NG2 cells. It was observed, however, that pericyte processes covered most of the capillary endothelium, consistent with reports that capillary pericytes in the central nervous system cover 70% to 85% of the microvessel endothelium.^{6,54}

In addition to capillary pericytes, we also observed characteristic labeling of vascular mural cells on arterioles and venules. Determining the basement membrane investment of these cells with electron microscopy was beyond the scope of this study; however, microscopy showed classic dense banding appearance of NG2 cells on arterioles. This patterning is identical to pericytes described with scanning electron microscopy (for review, see Shepro and Morel⁷), or vascular smooth muscle cells, as reviewed by Armulik et al.⁵³ Stellate cells showed sparse coverage on larger venules, different from both their capillary and arteriole counterparts. Stellate venule cells are believed to be vascular smooth muscle cells,^{1,53} although the distinction between these and pericytes are perhaps more subtle. The appearance of vascular mural cells on large vessels was similar to the morphology of vascular smooth muscle cells, as visualized with α -smooth muscle actin labeling (Supplementary Fig. S11). This report primarily focuses on NG2 cells on capillaries smaller than 7 μm , which

generally exhibit weak α -smooth muscle actin labeling and are morphologically consistent with pericytes measured with other techniques, such as trypsin digest.^{4,20,65}

Ruling Out Morphology of Other Labeled Cell Types

An added advantage of imaging the NG2 DsRed mouse is that oligodendrocyte progenitors are notably absent in the retina. In the brain, NG2 labeling is found to label oligodendrocyte progenitors, potentially confounding pericyte identification. Conversely, in the eye, the axons of the retinal ganglion cells are unmyelinated, meaning that oligodendrocyte progenitors are less confounding. Therefore, in the retina, NG2 labeling may have even greater pericyte labeling specificity without the need for further histological validation to rule out oligodendrocyte progenitors. Moreover, although NG2 expression can label neural/glial progenitor cells, it does not express in mature oligodendrocytes, astrocytes, resting microglia, or neurons (oral communication from Jackson Labs, 2012). Therefore, the fully developed retina in adult animals we imaged lack these alternate cell types. Perhaps most convincing was that the only labeled cells with soma observed were those directly in contact with the vascular endothelium. This uniquely vascular location and morphology of NG2 cells is altogether inconsistent with nascent oligodendrocytes, microglia, astrocyte, or neuron progenitor cells, which NG2 is also known to label. Given this evidence, we propose that using the NG2 DsRed mouse to study pericytes in the retina may provide an extra advantage over pericyte study in the brain using the same model, as labeling specificity is more closely confined to vascular associated cells.

The Role of Dynamic Pericyte Function

Future *in vivo* imaging of pericytes also may shed light on a contested debate in the circulation community; namely, do pericytes demonstrate contractility *in vivo*? NG2 antibodies were used to identify pericytes in a seminal study by Peppiatt et al.¹⁴ where the authors demonstrated pericyte contractility *in vitro*, thereby potentially mediating neurovascular coupling (the process by which active neurons signal to surrounding vasculature to dilate in order to serve metabolic need). However, validations of these reports have so far been confirmed only *in vitro*¹⁴ where blood perfusion dynamics are dramatically changed. *In vivo* observations of pericyte contractility have not been found.¹⁵ In this report, we provide a new model approach to test the neurovascular coupling hypothesis in the living eye, an extension of the central nervous system. This model may provide a more noninvasive approach to investigate whether capillary pericytes can mediate neurovascular coupling. The submicron resolution demonstrated by AOSLO may provide the necessary resolution needed to detect small-diameter changes associated with capillary vasodynamics. Future studies will investigate whether pericytes contract or dilate in response to visual stimulation and determine if blood flow changes accordingly.

Persistence of Label Throughout Adulthood

Phenotypically, DsRed animals cannot be distinguished from their nonexpressing littermates or normal C57BL6 animals of the same age. This suggests that the inserted BAC transgene is minimally invasive to normal systemic physiology; important for future considerations of this model for longitudinal study, especially in examining retinal vascular disease. To the benefit of longitudinal study, we found that adult mice (older than P44) maintained persistent fluorescent labeling in mural cells

of the vasculature throughout adulthood. The oldest animal imaged was 1.65 years of age, and was in good health at time of euthanasia. Both in vivo and postmortem histology confirm this finding despite some inconsistency with reports that suggest NG2 is expressed only in the developing vasculature.^{62,66} Our finding that NG2 is expressed throughout adulthood in the “mature” retinal vasculature inspires further discussion: are retinal NG2 cells a unique and quiescent population of potential progenitor cells in the retinal vasculature? Is this NG2 expression in the mature retina a unique feature of pericytes in the retina? Does it suggest a motile role or developmental role of these cells to dynamically move and regulate the retinal vasculature over time? These questions will be of high interest and posit important hypotheses to be tested in future experiments.

Toward many of these exciting avenues of research and more, the AOSLO also enables a multichannel imaging approach providing the ability to dynamically image NG2 pericytes and blood flow simultaneously and noninvasively throughout murine adulthood. This opens a new window of opportunity to study the retina pericyte in both its natural habitat, and perturbations of that habitat, that lead to health and disease of the microvascular network of the central nervous system.

Clinical Significance

Although the scope of the present proposal is confined to a mouse model, the simultaneous imaging of retinal blood flow and pericytes may fundamentally change the way we understand vascular-associated diseases of the retina. Diabetic retinopathy, for example, is one of the major complications of diabetes mellitus (a disease currently found in approximately 6% of the world population, with increasing annual incidence),⁶⁷ and is the leading cause of blindness in working age adults.^{68,69} Clinically, the proliferative stages of the disease are most damaging to vision as weak, angiogenic vessels grow, rupture, and leak, leaving occlusive exudates. However, the early stages of the disease that precede the proliferative stages are not well understood due to the microscopic nature of the primary cellular events associated with capillaries. Postmortem analysis reveals that loss of pericytes is one of the earliest morphological changes observed in diabetic subjects.^{4,20} However, the interpretation of this observation is still unclear.^{4,21,70} Are low pericyte numbers the cause or effect of another earlier associated event in diabetic retinopathy? Toward this line of investigation, we provide the first demonstration that pericytes can be imaged noninvasively with high resolution in the eye. This affords the unique opportunity to study the earliest events of pericyte loss, migration, and dropout associated with the initial stages of vascular disease in the same animal. For example, diabetic retinopathy may directly impact pericyte structure, compromising their putative role as a structural support for capillaries.⁷¹ Simultaneous noninvasive imaging of blood flow may facilitate this level of investigation.

Clues to date about what is the primary event in diabetic retinopathy have come from postmortem histology. Unfortunately, the only changes in capillary blood flow that can be inferred from histological observations are those associated with capillary dropout, and reductions in velocity, for example, cannot be detected. Recently, this difficulty has been overcome with in vivo studies in which contrast tracers have been injected, such as acridine orange to label leukocytes.^{72,73} However, questions remain whether this staining procedure “activates” leukocytes, changing their normal adherence to the endothelium.⁷³⁻⁷⁵ We have thus previously lacked the neces-

sary resolution to determine whether *all* blood cells in a vessel have stopped.⁷²⁻⁷⁴

Longitudinal study of the same animal over the course of disease has been notably lacking because of the need to perform ex vivo histology to acquire necessary resolution. Through adaptive optics, researchers may be able to better evaluate the early, preclinical stages of disease and lend insight to the primary cause(s) of vascular pathology. Identifying the earliest events may refine treatment strategies that target cellular mechanisms before retinopathy is prevalent, thereby improving on the invasive laser photocoagulation that is the standard of care for several vascular diseases of the eye today.

Acknowledgments

We thank Robin Sharma, Tracy Bubel, and Bill Fischer for their contributions to in vivo mouse imaging and histology support, and Robert Bell and Berislav Zlokovic for providing mice for pilot data in this project. Thanks also to Bill Merigan for manuscript review and project guidance.

Supported by National Institutes of Health (NIH) National Research Service Award F32EY023496, Center for Visual Science Training Fellowship NIH 5T32EY007125-22, Center for Vision Science Core Grant EY001319, Bioengineering Research Partnerships Grant EY014375, and Schmitt Program for Integrative Brain Research Fellowship.

Disclosure: **J. Schallek**, None; **Y. Geng**, None; **H. Nguyen**, None; **D.R. Williams**, Bausch and Lomb (F), Polgenix (F), Canon (F), Welch Allyn (F), Pfizer (C), P

References

1. Armulik A, Abramsson A, Betsholtz C. Endothelial/pericyte interactions. *Circ Res*. 2005;97:512-523.
2. Proebstl D, Voisin M-B, Woodfin A, et al. Pericytes support neutrophil subendothelial cell crawling and breaching of venular walls in vivo. *J Exp Med*. 2012;209:1219-1234.
3. Laties AM, Rapoport SI, McGlinn A. Hypertensive breakdown of cerebral but not of retinal blood vessels in rhesus monkey. *Arch Ophthalmol*. 1979;97:1511-1514.
4. Kuwabara T, Cogan DG. Retinal vascular patterns. VI. Mural cells of the retinal capillaries. *Arch Ophthalmol*. 1963;69:492-502.
5. Frank RN, Turczyn TJ, Das A. Pericyte coverage of retinal and cerebral capillaries. *Invest Ophthalmol Vis Sci*. 1990;31:999-1007.
6. Frank RN, Dutta S, Mancini MA. Pericyte coverage is greater in the retinal than in the cerebral capillaries of the rat. *Invest Ophthalmol Vis Sci*. 1987;28:1086-1091.
7. Shepro D, Morel NM. Pericyte physiology. *FASEB J*. 1993;7:1031-1038.
8. Armulik A, Genove G, Mae M, et al. Pericytes regulate the blood-brain barrier. *Nature*. 2010;468:557-561.
9. Winkler EA, Bell RD, Zlokovic BV. Pericyte-specific expression of PDGF beta receptor in mouse models with normal and deficient PDGF beta receptor signaling. *Mol Neurodegener*. 2010;5:32.
10. Darland DC, D'Amore PA. Blood vessel maturation: vascular development comes of age. *J Clin Invest*. 1999;103:157-158.
11. Stratman AN, Davis GE. Endothelial cell-pericyte interactions stimulate basement membrane matrix assembly: influence on vascular tube remodeling, maturation, and stabilization. *Microsc Microanal*. 2012;18:68-80.
12. Hughes S, Chan-Ling T. Characterization of smooth muscle cell and pericyte differentiation in the rat retina in vivo. *Invest Ophthalmol Vis Sci*. 2004;45:2795-2806.

13. Liu H, Zhang W, Kennard S, Caldwell RB, Lilly B. Notch3 is critical for proper angiogenesis and mural cell investment novelty and significance. *Circ Res*. 2010;107:860–870.
14. Peppiatt CM, Howarth C, Mobbs P, Attwell D. Bidirectional control of CNS capillary diameter by pericytes. *Nature*. 2006;443:700–704.
15. Fernández-Klett F, Offenhauser N, Dirnagl U, Priller J, Lindauer U. Pericytes in capillaries are contractile in vivo, but arterioles mediate functional hyperemia in the mouse brain. *Proc Natl Acad Sci U S A*. 2010;107:22290–22295.
16. Ogden CL, Carroll MD, Curtin LR, McDowell MA, Tabak CJ, Flegal KM. Prevalence of overweight and obesity in the United States, 1999–2004. *JAMA*. 2006;295:1549–1555.
17. Kempner JH, O'Colmain BJ, Leske MC, et al. The prevalence of diabetic retinopathy among adults in the United States. *Arch Ophthalmol*. 2004;122:552–563.
18. Centers for Disease Control and Prevention. Diabetes Public Health Resource. 2011 National Diabetes Fact Sheet. Available at: <http://www.cdc.gov/diabetes/pubs/factsheet11.htm>. Accessed August 15, 2013.
19. Fong DS, Aiello LP, Ferris FL, Klein R. Diabetic retinopathy. *Diabetes Care*. 2004;27:2540–2553.
20. Cogan DG, Toussaint D, Kuwabara T. Retinal vascular patterns. IV. Diabetic retinopathy. *Arch Ophthalmol*. 1961;66:366–378.
21. Hammes H-P, Lin J, Renner O, et al. Pericytes and the pathogenesis of diabetic retinopathy. *Diabetes*. 2002;51:3107–3112.
22. Liang J, Williams DR, Miller DT. Supernormal vision and high-resolution retinal imaging through adaptive optics. *J Opt Soc Am A Opt Image Sci Vis*. 1997;14:2884–2892.
23. Morgan JIW, Gray DC, Wolfe R, Masella B, Dubra A, Williams DR. Imaging individual human retinal pigment epithelium cells in vivo. *Invest Ophthalmol Vis Sci*. 2007;48:1953.
24. Roorda A, Williams DR. The arrangement of the three cone classes in the living human eye. *Nature*. 1999;397:520–522.
25. Geng Y, Dubra A, Yin L, et al. Adaptive optics retinal imaging in the living mouse eye. *Biomed Opt Express*. 2012;3:715–734.
26. Zhu X, Bergles DE, Nishiyama A. NG2 cells generate both oligodendrocytes and gray matter astrocytes. *Development*. 2008;135:145–157.
27. Dubra A, Harvey Z. Registration of 2D images from fast scanning ophthalmic instruments. In: Fischer B, Dawant BM, Lorenz C, eds. *Biomedical Image Registration*. Lecture Notes in Computer Science. Springer Berlin Heidelberg; 2010:60–71.
28. Alt C, Runnels JM, Teo GSL, Lin CP. In vivo tracking of hematopoietic cells in the retina of chimeric mice with a scanning laser ophthalmoscope. *IntraVital*. 2012;1:132–140.
29. Yin L, Geng Y, Osakada F, et al. Imaging light responses of retinal ganglion cells in the living mouse eye. *J Neurophysiol*. 2013;109:2415–2421.
30. Hill RA, Natsume R, Sakimura K, Nishiyama A. NG2 cells are uniformly distributed and NG2 is not required for barrel formation in the somatosensory cortex. *Mol Cell Neurosci*. 2011;46:689–698.
31. Ziskin JL, Nishiyama A, Rubio M, Fukaya M, Bergles DE. Vesicular release of glutamate from unmyelinated axons in white matter. *Nat Neurosci*. 2007;10:321–330.
32. Calderone L, Grimes P, Shalev M. Acute reversible cataract induced by xylazine and by ketamine-xylazine anesthesia in rats and mice. *Exp Eye Res*. 1986;42:331–337.
33. Geng Y, Schery LA, Sharma R, et al. Optical properties of the mouse eye. *Biomed Opt Express*. 2011;2:717–738.
34. Gomez-Vieyra A, Dubra A, Malacara-Hernandez D, Williams DR. First-order design of off-axis reflective ophthalmic adaptive optics systems using afocal telescopes. *Opt Express*. 2009;17:18906–18919.
35. Roorda A, Romero-Borja F, Donnelly I, Queener H, Hebert T, Campbell M. Adaptive optics scanning laser ophthalmoscopy. *Opt Express*. 2002;10:405–412.
36. Schmucker C, Schaeffel F. A paraxial schematic eye model for the growing C57BL/6 mouse. *Vision Res*. 2004;44:1857–1867.
37. Lyubarsky AL, Falsini B, Pennesi ME, Valentini P, Pugh EN. UV- and midwave-sensitive cone-driven retinal responses of the mouse: a possible phenotype for coexpression of cone photopigments. *J Neurosci*. 1999;19:442–455.
38. Applebury M, Antoch M, Baxter L, et al. The murine cone photoreceptor A single cone type expresses both S and M opsins with retinal spatial patterning. *Neuron*. 2000;27:513–523.
39. Morgan JIW, Hunter JJ, Masella B, et al. Light-induced retinal changes observed with high-resolution autofluorescence imaging of the retinal pigment epithelium. *Invest Ophthalmol Vis Sci*. 2008;49:3715–3729.
40. Morgan JIW, Hunter JJ, Merigan WH, Williams DR. The reduction of retinal autofluorescence caused by light exposure. *Invest Ophthalmol Vis Sci*. 2009;50:6015–6022.
41. Morgan JIW, Dubra A, Wolfe R, Merigan WH, Williams DR. In vivo autofluorescence imaging of the human and macaque retinal pigment epithelial cell mosaic. *Invest Ophthalmol Vis Sci*. 2009;50:1350–1359.
42. Baird GS, Zacharias DA, Tsien RY. Biochemistry, mutagenesis, and oligomerization of DsRed, a red fluorescent protein from coral. *Proc Natl Acad Sci U S A*. 2000;97:11984–11989.
43. Scheiner AJ, Riva CE, Kazahaya K, Petrig BL. Effect of flicker on macular blood flow assessed by the blue field simulation technique. *Invest Ophthalmol Vis Sci*. 1994;35:3436–3441.
44. Schallek J, Ts'o D. Blood contrast agents enhance intrinsic signals in the retina: evidence for an underlying blood volume component. *Invest Ophthalmol Vis Sci*. 2011;52:1325–1335.
45. Schallek J, Li H, Kardon R, et al. Stimulus-evoked intrinsic optical signals in the retina: spatial and temporal characteristics. *Invest Ophthalmol Vis Sci*. 2009;50:4865–4872.
46. Tam J, Martin JA, Roorda A. Noninvasive visualization and analysis of parafoveal capillaries in humans. *Invest Ophthalmol Vis Sci*. 2010;51:1691–1698.
47. Tam J, Tiruveedhula P, Roorda A. Characterization of single-file flow through human retinal parafoveal capillaries using an adaptive optics scanning laser ophthalmoscope. *Biomed Opt Express*. 2011;2:781–793.
48. Paques M, Tadayoni R, Sercombe R, et al. Structural and hemodynamic analysis of the mouse retinal microcirculation. *Invest Ophthalmol Vis Sci*. 2003;44:4960–4967.
49. Schmid B, Schindelin J, Cardona A, Longair M, Heisenberg M. A high-level 3D visualization API for Java and ImageJ. *BMC Bioinformatics*. 2010;11:274.
50. May CA, Lütjen-Drecoll E. Morphology of the murine optic nerve. *Invest Ophthalmol Vis Sci*. 2002;43:2206–2212.
51. Cuthbertson RA, Mandel TE. Anatomy of the mouse retina. Endothelial cell-pericyte ratio and capillary distribution. *Invest Ophthalmol Vis Sci*. 1986;27:1659–1664.
52. Bell RD, Winkler EA, Sagare AP, et al. Pericytes control key neurovascular functions and neuronal phenotype in the adult brain and during brain aging. *Neuron*. 2010;68:409–427.
53. Armulik A, Genové G, Betsholtz C. Pericytes: developmental, physiological, and pathological perspectives, problems, and promises. *Dev Cell*. 2011;21:193–215.
54. Zlokovic BV. The blood-brain barrier in health and chronic neurodegenerative disorders. *Neuron*. 2008;57:178–201.
55. Williamson JR, Tilton RG, Kilo C, Yu S. Immunofluorescent imaging of capillaries and pericytes in human skeletal muscle and retina. *Microvasc Res*. 1980;20:233–241.
56. Remtulla S, Hallett PE. A schematic eye for the mouse, and comparisons with the rat. *Vision Res*. 1985;25:21–31.
57. Nishiyama A, Komitova M, Suzuki R, Zhu X. Polydendrocytes (NG2 cells): multifunctional cells with lineage plasticity. *Nat Rev Neurosci*. 2009;10:9–22.

58. Wigley R, Hamilton N, Nishiyama A, Kirchhoff F, Butt AM. Morphological and physiological interactions of NG2-glia with astrocytes and neurons. *J Anat.* 2007;210:661-670.
59. Snodderly D, Weinhaus R, Choi J. Neural-vascular relationships in central retina of macaque monkeys (*Macaca fascicularis*). *J Neurosci.* 1992;12:1169-1193.
60. Huang F-J, You W-K, Bonaldo P, Seyfried TN, Pasquale EB, Stallcup WB. Pericyte deficiencies lead to aberrant tumor vascularization in the brain of the NG2 null mouse. *Dev Biol.* 2010;344:1035-1046.
61. Ruiter D, Schlingemann R, Westphal J, Denijn M, Rietveld F, De Waal R. Angiogenesis in wound healing and tumor metastasis. *Bebring Inst Mitt.* 1993;(92):258-272.
62. Ozerdem U, Grako KA, Dahlin-Huppe K, Monosov E, Stallcup WB. NG2 proteoglycan is expressed exclusively by mural cells during vascular morphogenesis. *Dev Dyn.* 2001;222:218-227.
63. Cogan DGKT. The mural cell in perspective. *Arch Ophthalmol.* 1967;78:133-139.
64. Hughes S, Gardiner T, Baxter L, Chan-Ling T. Changes in pericytes and smooth muscle cells in the kitten model of retinopathy of prematurity: implications for plus disease. *Invest Ophthalmol Vis Sci.* 2007;48:1368-1379.
65. Speiser P, Gittelsohn AM, Patz A. Studies on diabetic retinopathy. 3. Influence of diabetes on intramural pericytes. *Arch Ophthalmol.* 1968;80:332-337.
66. Nishiyama A, Lin X-H, Giese N, Heldin C-H, Stallcup WB. Colocalization of NG2 proteoglycan and PDGF α -receptor on O2A progenitor cells in the developing rat brain. *J Neurosci Res.* 1996;43:299-314.
67. Van den Oever IAM, Raterman HG, Nurmohamed MT, Simsek S. Endothelial dysfunction, inflammation, and apoptosis in diabetes mellitus. *Mediators Inflamm.* 2010;2010:792393.
68. Klein R, Klein BE, Moss SE, Davis MD, DeMets DL. The Wisconsin epidemiologic study of diabetic retinopathy. IV. Diabetic macular edema. *Ophthalmology.* 1984;91:1464-1474.
69. Klein R, Klein BEK, Moss SE, Davis MD, DeMets DL. The Wisconsin Epidemiologic Study of Diabetic Retinopathy: III. Prevalence and risk of diabetic retinopathy when age at diagnosis is 30 or more years. *Arch Ophthalmol.* 1984;102:527-532.
70. Hammes H-P, Lin J, Wagner P, et al. Angiopoietin-2 causes pericyte dropout in the normal retina. *Diabetes.* 2004;53:1104-1110.
71. Enge M, Bjarnegård M, Gerhardt H, et al. Endothelium-specific platelet-derived growth factor-B ablation mimics diabetic retinopathy. *EMBO J.* 2002;21:4307-4316.
72. Nishiwaki H, Ogura Y, Kimura H, Kiryu J, Honda Y. Quantitative evaluation of leukocyte dynamics in retinal microcirculation. *Invest Ophthalmol Vis Sci.* 1995;36:123-130.
73. Nishiwaki H, Ogura Y, Miyamoto K, Matsuda N, Honda Y. Interferon alfa induces leukocyte capillary trapping in rat retinal microcirculation. *Arch Ophthalmol.* 1996;114:726-730.
74. Miyamoto K, Khosrof S, Bursell SE, et al. Prevention of leukostasis and vascular leakage in streptozotocin-induced diabetic retinopathy via intercellular adhesion molecule-1 inhibition. *Proc Natl Acad Sci U S A.* 1999;96:10836-10841.
75. Schröder S, Palinski W, Schmid-Schönbein GW. Activated monocytes and granulocytes, capillary nonperfusion, and neovascularization in diabetic retinopathy. *Am J Pathol.* 1991;139:81-100.